Materials Today Bio 14 (2022) 100256

Contents lists available at ScienceDirect

Materials Today Bio

journal homepage: www.journals.elsevier.com/materials-today-bio

Design of a genetically programmed barnacle-curli inspired living-cell bioadhesive

Fei Li, Luona Ye, Longyu Zhang, Xiaoyan Li, Xiaoxiao Liu, Jiarui Zhu, Huanhuan Li, Huimin Pang, Yunjun Yan **, Li Xu, Min Yang, Jinyong Yan *

Key Lab of Molecular Biophysics of Ministry of Education, College of Life Science and Technology Huazhong University of Science and Technology, Wuhan, China

ARTICLE INFO

Keywords:
Barnacles
Biofilms
Self-assembly
Genetic engineering
Bioadhesives

ABSTRACT

In nature, barnacles and bacterial biofilms utilize self-assembly amyloid to achieve strong and robust interface adhesion. However, there is still a lack of sufficient research on the construction of macroscopic adhesives based on amyloid-like nanostructures through reasonable molecular design. Here, we report a genetically programmed self-assembly living-cell bioadhesive inspired by barnacle and curli system. Firstly, the encoding genes of two natural adhesion proteins (CsgA and cp19k) derived from *E. coli* curli and barnacle cement were fused and expressed as a fundamental building block of the bioadhesive. Utilizing the natural curli system of *E. coli*, fusion protein can be delivered to cell surface and self-assemble into an amyloid nanofibrous network. Then, the *E. coli* cells were incorporated into the molecular chain network of xanthan gum (XG) through covalent conjugation to produce a living-cell bioadhesive. The shear adhesive strength of the bioadhesive to the surface of the aluminum sheet reaches 278 kPa. Benefiting from living cells encapsulated inside, the bioadhesive can self-regenerate with adequate nutrients. This adhesive has low toxicity to organisms, strong resistance to the liquid environment in vivo, easy to pump, exhibiting potential application prospects in biomedical fields such as intestinal soft tissue repair.

1. Introduction

Nowadays, biocompatible, processable and strong adhesives are highly demanded both in industrial and biomedical fields, such as tissue adhesives and hemostatic materials [1]. Interestingly, several natural organisms such as mussels, barnacles, bacterial biofilms and marine flatworms have provided a wealth of inspiration for the manufacture of biomimetic adhesives [2]. To date, a large number of biomimetic adhesives based on marine bioadhesion systems have been developed. Hybrid materials that combine two or more independent natural adhesion systems have the potential to combine the advantages of different systems and are therefore attractive. Recently, some researchers have used genetic engineering methods to produce recombinant proteins expressed by fusion of mussel foot protein (Mfp) and bacterial curli, which have an underwater adhesion energy approaching 20.9 mJ m^{-2} [3]. However, although these materials are designed in cells, they do not fully exploit the characteristics of living biological systems, and their purification process is complex and the yield is low, which cannot meet the needs of practical applications.

Through synthetic biology techniques, living cells can be engineered into tunable multiscale materials with programmable properties of living systems such as self-regeneration and environmental responsiveness, which provides new ideas for the development of biomimetic adhesives [4]. As the major proteinaceous component of enteric biofilms of *E. coli* and *Salmonella*, curli is a typical example of functional adhesive amyloids, which can be used as a protein scaffold to synthesize various hybrid materials [5]. Some researchers have used the Mfp domains to functionalize curli on cell surface, thus making bacterial biofilm into living glues [6]. However, the currently reported mussel-inspired living glue system relies on the action of tyrosinase, which requires the use of high concentrations of Cu (II) to ensure the enzyme activity, which limits its practical application [7].

Barnacle cement is another attractive natural adhesion system. Barnacles can tenaciously adhere to a wide range of underwater substrates by secreting and curing multiple protein components which are integrated into amyloid-like nanofibrous network and eventually form a

* Corresponding author.
** Corresponding author.
E-mail addresses: yanyunjun@hust.edu.cn (Y. Yan), yjiny@126.com (J. Yan).

https://doi.org/10.1016/j.mtbio.2022.100256
Received 28 December 2021; Received in revised form 3 April 2022; Accepted 5 April 2022
Available online 8 April 2022

highly insoluble cement material [8]. In amyloid nanofibers, the β chain is oriented perpendicular to the fibril axis and connected by a dense hydrogen bond network to form a supramolecular β sheet, which increases the contact area of peptide chains to substrates and improve the adhesive ability [9]. A 19 kDa protein (cp19k) found at the barnacle cement-substrate boundary is considered to play the key surface coupling role [10]. The primary structure of cp19k has been revealed, which contains two alternating blocks, one of which is dominated by Gly, Ser, Thr, Val and Ala residues, and the other is rich in hydrophobic and charged amino acids [11]. The unique molecular design of amino acids has been proven to endow cp19k with high interfacial activity and enable it to self-assemble into amyloid fibrils in seawater analogs, exhibiting higher adhesion than before self-assembly [12]. Recently, some researchers have used engineered *E. coli* curli as a host system to display barnacle adhesion component AACP43, which can be exported through the periplasmic space and aggregated into fibrous structures in the biofilm [13]. Therefore, the use of barnacle cement protein-functionalized curli system is expected to make a new type of living glue.

The curli on surface of engineered cells can also be used to synthesize functional composites with other inorganic or organic materials, such as minerals or metals, to enrich its applications [14,15]. Xanthan gum (XG) is an extracellular anionic polysaccharide purified from *Xanthomonas* [16]. XG has an ordered secondary structure under certain conditions, and its conformation has been identified as a network formed by self-assembly of interlaced molecular chains connected through dense hydrogen bonds, in which each single chain is formed with an intrinsic double-stranded helix [17]. Benefiting from this network structure, XG gels in aqueous solution, and its viscosity can reach more than 10^5 mPa s at low shear rate, exhibiting good thickening properties [18]. Moreover, the rich hydroxyl groups of XG provide possible sites for chemical modification and crosslinking [19]. Therefore, XG has the potential as one of the raw materials to improve the adhesion and viscoelasticity of hybrid adhesives.

In view of the similar self-assembly capabilities of the three bioadhesive materials, it is theoretically possible to use barnacle cp19k, *E. coli* curli and XG to develop stronger hybrid adhesives than single component. In this research, we have designed a bioinspired self-assembly living-cell adhesive (Fig. 1). Specifically, cp19k and CsgA recombinant proteins are fused and expressed in *E. coli* to work as a fundamental building block. Here, CsgA not only plays a role in accelerating amyloid self-assembly, but also acts as a platform to display recombinant protein on the *E. coli* cell surface and form a hierarchically assembled network of amyloid nanofibers. Then, we incorporated the *E. coli* cells into the network of XG via an amidation reaction, and used XG as the matrix forming material of the bioadhesive. The engineered *E. coli* cells fixed inside the living-cell bioadhesive can serve as a living factory which give it extraordinary properties such as genetic programmability and self-regeneration.

2. Material and methods

2.1. Strains and plasmids

E. coli DH5α and BL21 (DE3) ΔCsgA were employed for amplification of recombinant plasmids and protein production, respectively. BL21 (DE3) ΔCsgA is a mutant strain with deletion of CsgA gene, which was constructed frome BL21 (DE3) via the CRISPR-Cas9 system using plasmids pCas and pTargetF [20]. Genes of cp19k (from *Balanus albicostatus*) and CsgA (from *E. coli*) were synthesized and fused with a GS linker. Recombinant gene fragment CsgA-cp19k were cloned into the pET-28a (+) and pET-22b (+) vectors for protein expression and curli formation, respectively. Similarly, the gene fragments of CsgA and cp19k were respectively sub-cloned into the pET-28a (+) and pET-22b (+). Various molecular genetic manipulation regents and kits were bought from Beijing Solarbio Science & Technology Co., Ltd. (China). All standard substrates and other regents were purchased from TCI (Shanghai) Development Co., Ltd.

2.2. Protein expression and purification

The BL21 (DE3) ΔCsgA strain was transformed with pET-28a/CsgA, pET-28a/cp19k or pET-28a/CsgA-cp19k plasmids, respectively. These

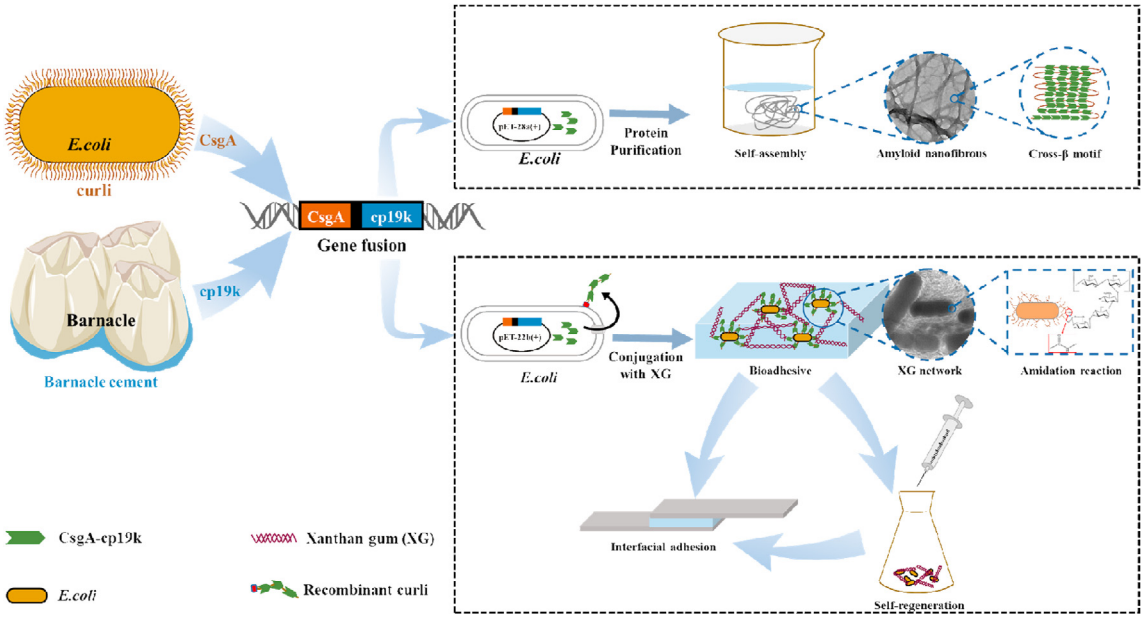

Fig. 1. Schematics of the modular design strategy for engineering the bioinspired living-cell adhesive. The development of artificial bioadhesive is inspired by two independent natural adhesion systems-*E. coli* curli and barnacle cement. The genes of two kinds of natural adhesion elements (CsgA and cp19k) were fused and cloned into the pET-28a (+) and pET-22b (+) vectors for protein purification and curli formation, respectively. When incubated in vitro, the purified protein CsgA-cp19k can self-assemble into amyloid nanofibers and shows a strong surface binding strength. When delivered to the extracellular area, CsgA-cp19k can form a recombinant curli network on cell surface. By conjugation with XG, curli-producing *E. coli* cells can be processed into a living-cell bioadhesive, which can self-regenerate under suitable conditions.

strains were grown until the OD_{600} = 0.6–0.9 in Luria-Bertani (LB) broth and then induced with 0.5 mM IPTG at 37 °C for 3 h. Following the growth, cells were harvested with centrifugation. The purification was performed under denaturing conditions to prevent premature self-assembly. Cell pellets were suspended in 50 mM phosphate buffer (pH = 7.2) that contained 8 M GdnHCl and incubated overnight at 4 °C to lyse the cells. After removal of the insoluble portions by centrifuging, the supernatants were incubated with the nickel-nitrilotriacetic acid (NI-NTA) resins for 2 h before the mixture was loaded onto the column. The resins were thoroughly washed with 50 mM phosphate buffer (pH = 7.2) before washed with 50 mM phosphate buffer that contained 50 mM imidazole and eluted with 50 mM phosphate buffer that contained 150 mM imidazole. The purified proteins were dialyzed against ultrapure water or artificial seawater (ASW, pH = 8.0) for 2 days to remove GdnHCl and then stored at 4 °C.

2.3. Thioflavin T (ThT) and circular dichroism (CD) assay

Purified and dialyzed proteins were loaded on 96-well black plates with transparent bottoms. ThT was added to a concentration of 20 μM. Fluorescence was measured by a FlexStation 3 multi-mode microplate reader set to 438 nm excitation and 495 nm emission with a 475 nm cutoff.

Circular dichroism (CD) spectra were recorded using a Jasco J-810 spectrometer at 25 °C in a quartz cell from 190 to 240 nm with the following parameters: 1 nm bandwidth, 1 s response, 500 nm/min scanning speed, and 0.1 cm path length. The protein samples were dialyzed against pure water for 24 h. The final concentration of protein samples prior to testing was adjusted to 1 mg/ml. The CD intensity was given as mean residue molar ellipticity (θ [deg × cm^2 × $dmol^{-1}$]).

2.4. QCM-D assay

The adsorption capacity of proteins on the silica surface was measured using QCM-D (Q-Sense E1). The QCM-D sensor surface rinsed with pure water until the frequency and dissipative signals reach equilibrium. The concentration of purified proteins was normalized to 2 mg/ml, and then the protein solution was flowed into the QCM-D flow cell at a rate of 20 μL/min. After incubated for 20 min, the sensor surface was rinsed again with pure water for to remove unbound or weakly bound soluble proteins. Frequency variation (ΔF) and dissipation (ΔD) were measured simultaneously at six overtones (n = 3, 5 … 13). These experiments were performed 3 times per sample.

2.5. Curli formation and yield quantification

To produce curli, BL21 (DE3) ΔCsgA cells were transformed with pET-22b/CsgA and pET-22b/CsgA-cp19k recombinant plasmids. As a negative control, BL21 (DE3) ΔCsgA cells were transformed with an empty pET-22b plasmid. After growth in LB liquid media supplemented with 100 mg ml^{-1} of ampicillin and 0.5 mM of IPTG for 48 h at 25 °C, the cells were streaked onto LB plates supplemented with 100 mg ml^{-1} ampicillin, 25 mg ml^{-1} Congo Red, and 5 mg ml^{-1} Brilliant Blue G-250 detect curli formation.

Curli on the cell surface was quantified by a whole-cell Congo red depletion assay [21]. Whole-cell samples were suspended in PBS with 10 μg/ml Congo Red and diluted to OD_{600} = 1.0. The cells were incubated with CR for 10 min at room temperature before pelleted, and the OD_{500} of the supernatant was measured on a spectrophotometer. Congo red depletion was defined as the difference between the OD_{500} of the PBS with 10 μg/ml Congo Red minus the OD_{500} of the supernatant, which was used to quantify the curli yield. Each sample was prepared and assayed in triplicate.

2.6. Western blotting

The expression of curli consisting of CsgA or CsgA-cp19k was verified by western blotting assay as reported [22]. After induced to form curli, the cell cultures of BL21 (DE3) ΔCsgA transformed with empty plasmid, pET-22b/CsgA or pET-22b/CsgA-cp19k were centrifuged to obtain whole cell pellets, then resuspended in PBS and normalized by cell density to OD600 = 0.5. Then 1 ml of each pellet was treated with 100 μL of hexafluoro isopropanol (HFIP) as indicated to dissociate the curli subunits. HFIP was removed by vacuum centrifugation, and the samples were resuspended in SDS-PAGE loading buffer and subjected to protein gel electrophoresis, followed by transfer to PVDF membranes (Roche, USA). Mouse anti-6 × Histag antibody used as primary antibody and goat anti-mouse IgG-HRP was used as secondary antibody, and a DAB Substrate Kit was used for color development.

2.7. Immunofluorescence detection test

After induction of curli generation, cell pellets were washed twice with PBS buffer. A small amount of cells were resuspended a in 50 μl of PBS buffer containing 1 mg/ml BSA, added with 1 μl of mouse anti-6 × Histag primary antibody and incubated in a 28 °C water bath for 3 h. The cells were then washed with PBS buffer and resuspend in 50 μl of PBS buffer containing 1 mg/ml BSA, added with 1 μl of FITC-labeled goat anti-mouse secondary antibody, mix well, and incubate at 28 °C for 2 h in the dark. After washing the cells with PBS buffer, samples were taken and observed under a fluorescence microscope, with 488 nm excitation light.

2.8. Glass bonding experiment

Glass binding assays were used to characterize cell surface binding capacity. The cells were loaded on a glass slide, kept for 2h, and then immersed in pure water and washed with a magnetic stirrer for 24 h. The number of cells that were loaded before washing and retained after washing were recorded. The relative surface binding capacity is quantified as the number of cells retained on the slide after washed for 24 h divided by the number of cells loaded on the slide. The number of cells on the slide was calculated by averaging the number of cells in 5 microscopic fields.

2.9. Transmission electron microscopy (TEM)

Bright-field TEM images were collected on a HT7700 HITACHI Transmission Electron Microscope. The samples were rinsed with 0.1 M, pH = 7.0 phosphate buffer and then dried by graded ethanol dehydration (60%, 70%, 80%, 90%, and 100% ethanol). The copper grids are placed on the droplet for 1 min, and then transferred to a filter paper sheet to dry the sample. Once dried, samples were negatively stained with 2 μl 0.3 wt % uranyl acetate.

2.10. Scanning electron microscopy (SEM)

The cell samples were fixed in 2.5% glutaraldehyde solution at 4 °C before rinsed with 0.1 M, pH = 7.0 phosphate buffer and then dried by graded ethanol dehydration before drop cast on silica substrates. The samples were sputter-coated with gold for 10 s before observation. The surface morphology of the coatings was observed with a field emission scanning electron microscope (Gemini SEM300).

2.11. Conjugation of XG and E. coli cells

5 ml 2.5 % wt XG aqueous solution were prepared by dissolving XG powder in deionized water and stir overnight. Then, EDC and NHS equal to the molar ratio of carboxyl groups in XG (2 mol of carboxyl groups per mole of XG) were added to the XG aqueous solution and the mixed solution was stirred at room temperature for 2 h to activate the carboxyl

groups of XG. The cell pellets were obtained from curli-producing cultures through centrifugation. Then cell pellets of different wet weights were added to the mixed solution. The entire solution was stirred for 4 h and then dialyzed for 1 d using dialysis membranes before stored at 4 °C.

2.12. The rheological properties of the living adhesives

Oscillatory rheology measurements of adhesives were performed on a rheometer (Anton Paar, Physical MCR 302) with a flat parallel plate (25 mm, diameter). The linear viscoelastic region was measured by a strain sweep measurement from a strain amplitude of 0.1%–300% at 25.0 °C (±0.1 °C) and a frequency of 10 Hz. The shear-thinning property of XG or XG-cell adhesive was investigated by measuring the viscosity at shear rates from 0.1 to 500 s^{-1}.

2.13. Lap shear measurement

The adhesion properties of the adhesives were evaluated using the lap shear test. Adhesive samples were evenly coated between two aluminum or glass sheets (25 × 100 × 2 mm), with an overlapping area of 25 × 30 mm. Then, the two sheets bonded with the adhesive sample were incubated at 37 °C for 24 h, and then the measurement was performed on a WDW-2 microcomputer controlled electronic universal testing machine.

2.14. Regeneration of living cell adhesives

Adhesives stored at 4 °C were re-seeded in LB medium containing 0.5 mM IPTG and incubated at 25 °C, 100 rpm for 24 h. Curli yield at 24th hour was quantified by a whole-cell Congo red depletion assay as before. Then cells were concentrated by centrifugation and conjugated with XG via an amide reaction. The adhesive was regenerated for 5 times by the same method, and the number of viable cells (CFU/ml) in the adhesive before and after regeneration was detected by diluting and coating on LB plate. The adhesion properties of the 1–5 generations of regenerated adhesives were evaluated using the lap shear test as before.

3. Results and discussion

3.1. Expression of recombinant proteins and characterization of in vitro self-assembly

CsgA, cp19k and their fusion protein CsgA-cp19k were expressed in *E. coli* BL21 (DE3) ΔCsgA cells. The CsgA and CsgA-cp19k proteins were obtained at a yield of about 50 mg/L, and cp19k was obtained at a higher yield of about 160 mg/L. The SDS-PAGE result shows single bands, and the molecular weight is consistent with the prediction (Fig. 2a). After 24 h of dialysis against ultrapure water or artificial sea water (ASW), the soluble proteins begin to aggregate into insoluble amyloid fibrils. Circular dichroism studies (Fig. S3) showed that both CsgA and CsgA-cp19k proteins dialyzed in pure water were enriched in β-sheet secondary structure with spectral minimums around 220 nm and maximums around 200 nm. Whereas a minimum around 200 nm can be observed in the cp19k spectrum, which is characteristic of random coil conformations. The shape of the CsgA-cp19k curve is slightly different from that of CsgA, possibly due to the unstructured features of the cp19k domain displayed outside the amyloid core. Thioflavin T (ThT) assay which probes for the β-sheet-rich structures of amyloid fibrils was used to monitor the in vitro self-assembly of proteins [23]. The self-assembly efficiencies of proteins

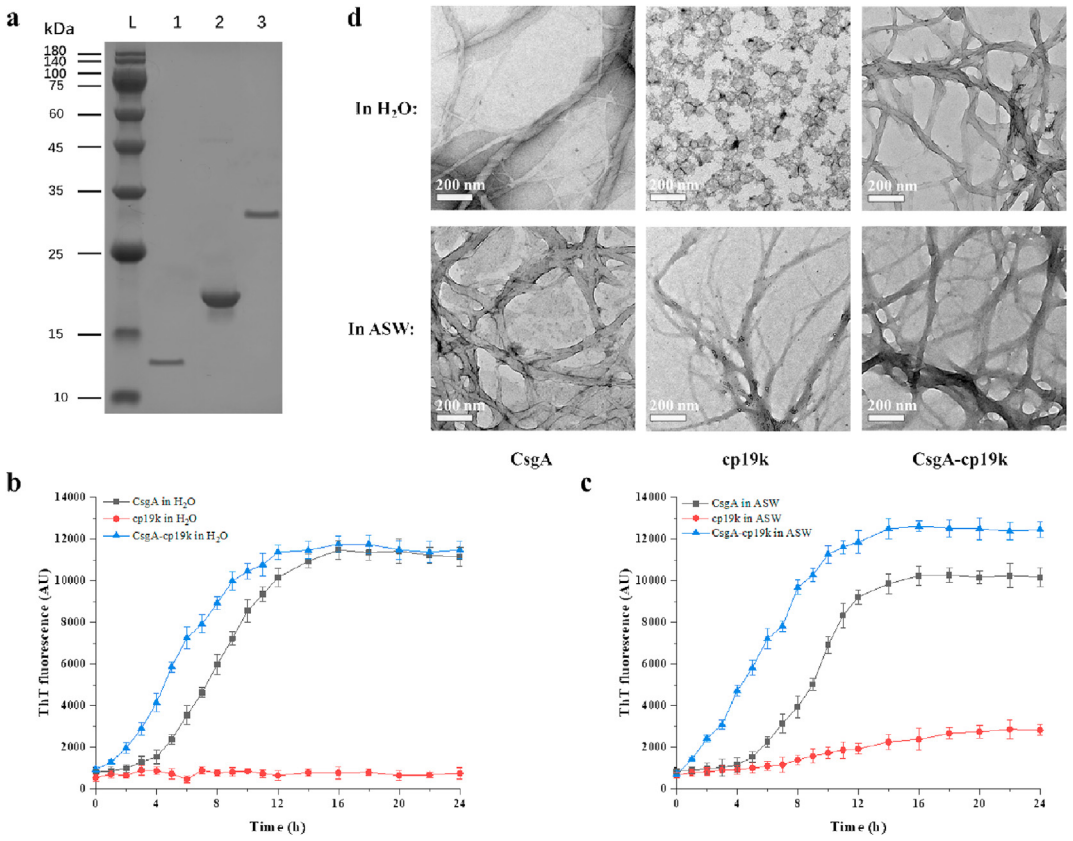

Fig. 2. Expression of recombinant proteins and characterization of in vitro self-assembly by ThT assay and TEM observation. **a**) SDS-PAGE gel verifies purification of the recombinant proteins purified by nickel-nitrilotriacetic acid (NI-NTA)-resin columns. Lane L, prestained protein ladder; lane 1, CsgA; lane 2, cp19k; lane 3, CsgA-cp19k. **b**) and **c**) The figures showing the relationship between Tht fluorescence (AU) of CsgA, cp19k and CsgA-cp19k proteins and time when incubated in ultrapure water or ASW. d) Transmission electron microscope (TEM) microscopic observation images of CsgA, cp19k and CsgA-cp19k proteins incubated in ultrapure water or ASW.

in pure water and ASW were detected according to the Thioflavin T fluorescence signal, respectively. As shown in Fig. 2, the assembly of cp19k occurs in ASW instead of pure water, indicating that cp19k requires a specific environment to trigger its amyloid formation tendency. This result is consistent with previous researchers who found that the recombinant cp19k can aggregate into typical amyloid fibrils in seawater analog [24]. In contrast, the ThT fluorescence curves of CsgA and CsgA-cp19k both rise rapidly and then reach a plateau after 12 h (Fig. 2b). In addition, the polymerization lag phase of Csga-cp19k is shorter than that of CsgA, which indicates that the fusion of the 19k domains accelerates the formation of amyloid. This phenomenon may be because unstructured cp19k domains enhance the efficiency of protein folding through the fly-casting mechanism, which assumes that relatively unstructured proteins can have a greater capture radius and increase protein folding rates by exploiting the available folding free energy [25].

The morphological characteristics of in vitro purified proteins were further observed with transmission electron microscopy (TEM) (Fig. 2d). For cp19k, the protein appears as dispersed spherical particles in ultrapure water, while in ASW, short and slim fibrils (about 20–30 nm in diameter) are formed and converge into larger aggregates. Different from cp19k, CsgA and CsgA-cp19k produce a large number of fibrils with significantly higher diameter (about 40–60 nm in diameter) and fiber length, which hierarchically assemble into dense nanofiber networks in both ultrapure water and ASW. The TEM results are consistent with the ThT determination, which proves that the fusion with the CsgA domain improves the self-assembly ability of cp19k.

3.2. Characterization of surface binding ability of recombinant proteins

In order to evaluate the surface binding ability of the purified proteins, a test was performed on quartz crystal microbalance with dissipation monitoring (QCM-D). The changes in frequency (ΔF) can reflect the amount of protein adsorbed on the silica surface. Compared with CsgA, the ΔF of cp19k and CsgA-cp19k dropped sharply in a short period of time, indicating that the latter two were absorbed on the silica surface and reached the adsorption equilibrium more rapidly (Fig. 3a). As reported, the biased amino acids in cp19k, including Thr, Ser, Ala, Val, and Lys, are particularly useful for coupling to silica surfaces via hydrogen bonding, hydrophobic interactions, and electrostatic interactions [26]. This explains the higher binding efficiency of CsgA-cp19k and cp19k to the silica surface in the test.

In addition, changes in dissipation (ΔD) can reflect viscoelasticity and stiffness of protein adsorption layers [27]. The $|\Delta D/\Delta F|$ value were used to characterize the viscoelasticity of the three protein adsorption layers. As shown in Fig. 3c, the $|\Delta D/\Delta F|$ value of cp19k was the highest and the change before and after rising was the largest, indicating that the structure of the protein adsorption layer was relatively loose and most proteins were reversibly adsorbed. Relatively speaking, the adsorption layers of CsgA and CsgA-cp19k were close to rigid, indicating that proteins in form of amyloid fibrils were more likely to form a dense structure on the silica surface, and thus were more difficult to desorb.

On the one hand, CsgA-cp19k can display more functional acid residues on the nanofibers by assembling into amyloid fibrils, which increases the contact area and promote non-covalent bonding with the substrate surface. On the other hand, the tape-like monomeric amyloids structure of CsgA and CsgA-cp19k may contribute to irreversible adhesion, because the formation of hinge during the desorption of nanofibers leads to an increase in peeling work [28]. This unique molecular design produces a synergistic effect to enhance adhesion performance.

3.3. Formation of recombinant curli and verification of the adhesion

Utilizing the natural mechanism of curli biogenesis in *E. coli*, we successfully delivered CsgA-cp19k to the cell surface and verified the formation of recombinant curli by an immunofluorescence detection test (Fig. 4a), where green fluorescence was observed on cells expressing CsgA-cp19k and CsgA, indicating that the recombinant proteins were displayed on the cell surface and bound to fluorescent antibody via His-tag. Congo Red (CR) staining assay also confirmed the expression of curli (Fig. 4d). The protein composition of the curli was verified by western blotting using *anti*-histag antibody, and the molecular weights of the bands were consistent with the monomeric proteins, demonstrating that curli consisted of CsgA or CsgA-cp19k recombinant proteins, respectively (Fig. 4e). The yield of curli was quantified by a whole-cell Congo red depletion assay and the curve of curli yield versus time was plot in Fig. 4f. Based on this curve, an induction time of 48 h was chosen to control the same yield of curli produced by CsgA-cp19k and CsgA in the following experiments. Furthermore, we morphologically observed the curli structures around *E. coli* cells with both transmission electron microscopy (TEM) and scanning electron microscopy (SEM) (Fig. 4b and c). In both TEM and SEM images, dense nanofibrous networks were observed around cells expressing CsgA-cp19k and CsgA, while no fibrous structures were found in the control group (empty plasmid transformation). These results confirm that CsgA-cp19k can be delivered to the cell surface and involved in the formation of curli.

The interfacial adhesion ability of recombinant *E. coli* was verified by glass surface bonding experiment. As shown in Fig. 4g, compared with the control group, the CsgA-cp19k and CsgA groups had significantly more recombinant cells remaining on the slide. Further quantitative analysis in Fig. 4h showed that the cells expressing CsgA-cp19k had stronger surface binding capacity. The experimental results proved that the interfacial adhesion ability of *E. coli* cell can be effectively improved by delivering the recombinant protein to the cell surface and forming a fibrous network, which provides a basis for the manufacture of the bioadhesive.

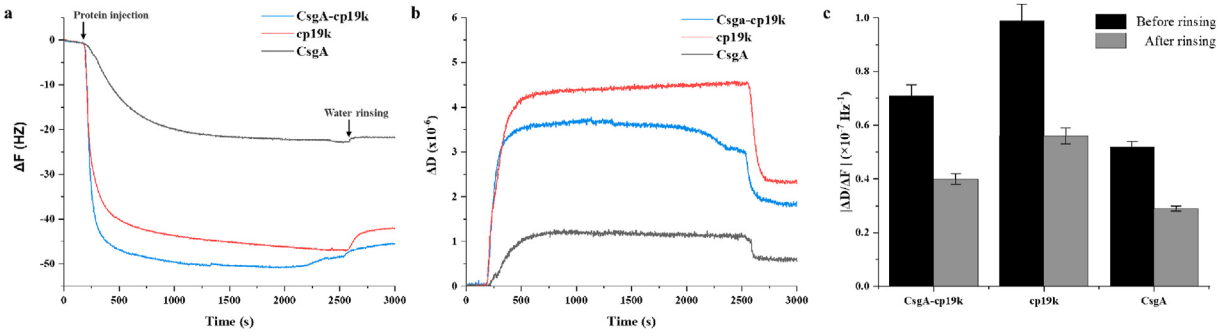

Fig. 3. Evaluation of surface binding ability based on molecular interface interaction between protein and silica through QCM-D experiments. a) The frequency change (ΔF/n for overtone n = 3) and time curves of CsgA, cp19k and CsgA-cp19k proteins. b). The dissipation change (ΔD) and time curves of CsgA, cp19k and CsgA-cp19k proteins. c). The $|\Delta D/\Delta F|$ value of CsgA, cp19k and CsgA-cp19k proteins at adsorption equilibrium before and after rinsing with pure water.

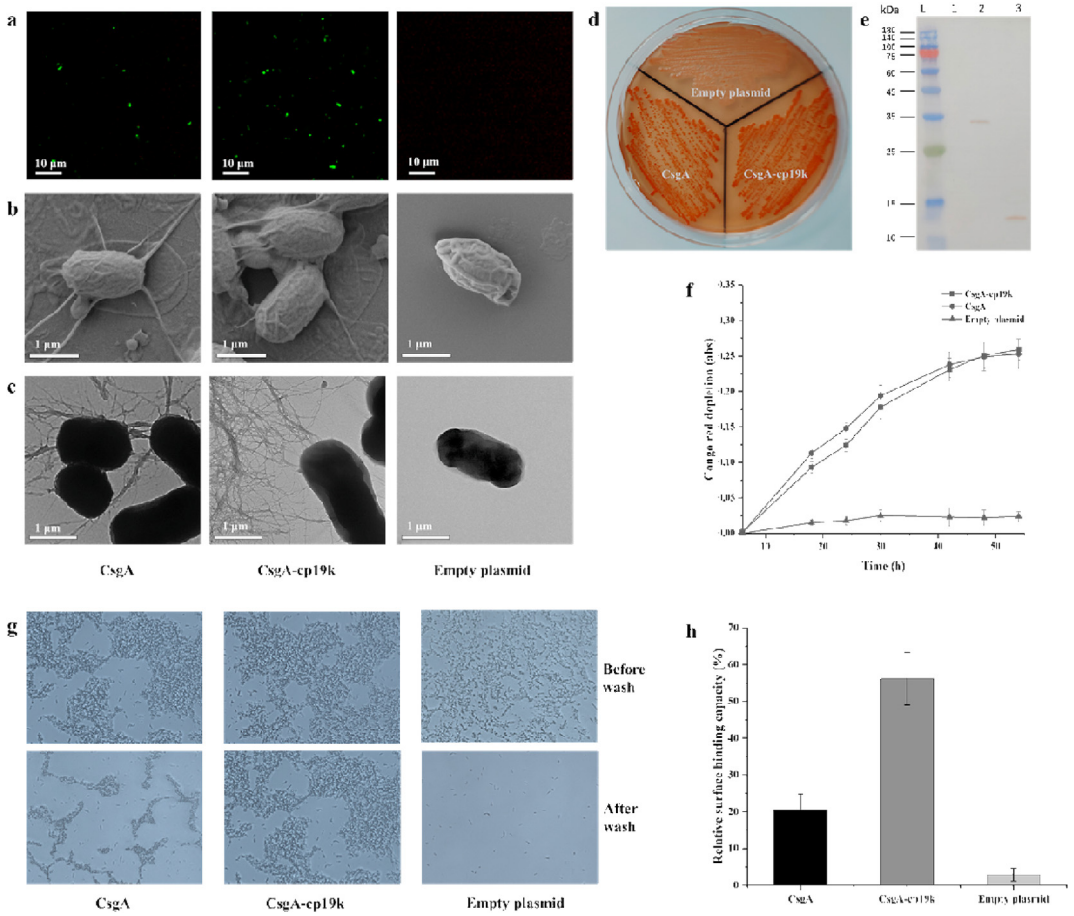

Fig. 4. Formation of recombinant curli was verified and the cell adhesion ability was confirmed by surface binding test. **a**) Images of engineered *E. coli* cells conjugated with fluorescent antibody under fluorescence microscope, with 488 nm excitation light. **b**) and **c**) scanning electron microscopy (SEM) and transmission electron microscopy (TEM) microscopic images of BL21 (DE3) ΔCsgA cells with pET-22b/CsgA, pET-22b/CsgA-cp19k or empty plasmid. **d**) Congo Red (CR) staining test on a LB plate. BL21 (DE3) ΔCsgA cells harboring pET-22b/CsgA, pET-22b/CsgA-cp19k or empty plasmid were coated on different areas of the plate. **e**) Curli expression consisting of CsgA or CsgA-cp19k was confirmed by western blotting using *anti*-histag antibody. Lane L, prestained protein ladder; lane 1: empty plasmid control; lane 2, CsgA-cp19k; lane 3, CsgA. **f**) The curve of curli yield versus time in BL21 (DE3) ΔCsgA cells harboring pET-22b/CsgA, pET-22b/CsgA-cp19k or empty plasmid by a whole-cell Congo red depletion assay. **g**) The cells that were loaded on glass slides before washing and retained after washing in the glass binding assays. **h**) Characterization of cell binding capacity by quantifying the remaining cells on the slide. (**) $P < 0.01$. Error bars indicate s.d.

3.4. Production and characterization of the living-cell bioadhesive

As reported, there are hypothesized enzyme-catalyzed polymerization reactions between the proteins in barnacle cement, which enables self-assembled nanofibers to generate fibrous bulk cement through covalent cross-linking for further curing, thereby improving the cohesion of barnacle cement and the adhesion strength to the interface [29]. Here, we covalently conjugated *E. coli* cells and XG through an amidation reaction to form a denser cross-linked network, thus producing a living-cell adhesive (Fig. 5a). Through TEM and SEM observation in Fig. 5, it was found that XG forms a dense network based on ordered double helix structure in aqueous solution. The network structure of XG was retained in the XG-cell adhesive, and a large number of XG chains were conjugated around the cell surface, which incorporate the cells into the cross-linked network. In order to verify the covalent conjugation of cells and XG, XG was directly mixed with cells as a control group, and the adhesives were repeatedly washed with pure water on the microporous membrane. As shown in Fig. 5b, no residual XG was observed on cells after adequate washing in the directly mixed control group, while XG in the CsgA-cp19k and CsgA groups was still clearly bound to cells. In addition, no significant residual XG was observed in the empty plasmid control without curli. The SEM observation in Fig. 5c also showed a similar phenomenon, indicating that curli plays a key role in the covalent conjugation of XG.

Rheological analysis revealed the influence of XG and curli on properties of the bioadhesive. Due to the network structure, XG exhibit weak gel-like and shear-thinning in aqueous solution [30]. The rheological analysis results in Fig. 5d showed that XG–cell adhesives retained the weak gel property of XG. The value of G′ in the figure is higher than the value of G”, indicating that the adhesives exhibit strong elastic properties. Significant differences in storage modulus were also observed between adhesives with different curli protein compositions. Compared to controls XG-EP and XG-CsgA, the G′ value of CsgA-cp19k adhesive was stronger, and it increased with the increase of cell content. This indicate that the rich amino acids of cp19k additional coupling sites and hydrogen bonds to XG, thereby enhancing the intermolecular association and increasing the cross-linking density (Fig. 5d). As shown in Fig. 5e, XG-cell adhesives exhibit similar shear thinning behavior and good thixotropy as XG, which enables it to be pumped by injection under shear stress, thus facilitating practical applications.

We further characterized the interface adhesion strength of XG-cell bioadhesive to aluminum or glass plates using a lap shear test on a universal tensile testing machine. As shown in Fig. 6a, the bioadhesives prepared with CsgA-cp19k expressing *E. coli* cells exhibited significant higher adhesive strength than the control groups, and the adhesive strength increased with the increase of cell concentration, reaching a maximum of 278 kPa on the surface of the aluminum sheet, indicating

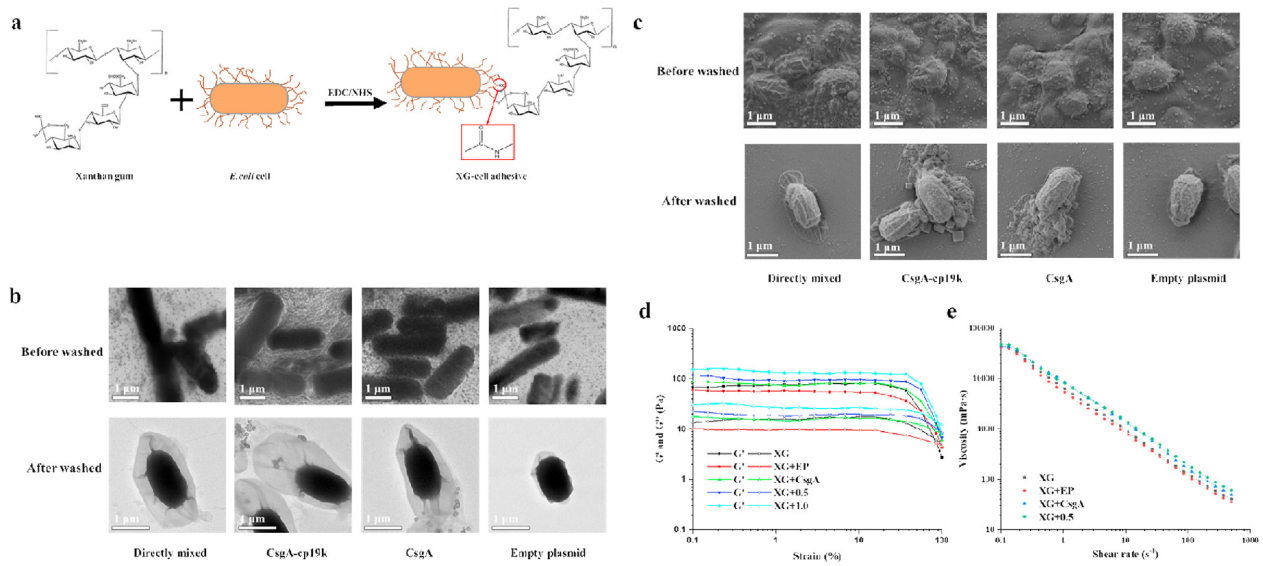

Fig. 5. Synthesis and rheology analysis of XG-cell bioadhesive. **a**) Synthesis of XG-cell bioadhesive through an amidation reaction. **b**) Transmission electron microscopy (TEM) microscopic images of XG-cell bioadhesives before and after adequate washing with pure water with a directly mixed control. **c**) Scanning electron microscopy (SEM) microscopic images of XG-cell bioadhesives before and after adequate washing with pure water with a directly mixed control. **d**) Strain sweep of shear rheology of XG and XG-cell bioadhesives (XG-EP and XG-CsgA stand for the adhesives prepared with XG and *E. coli* cells with a wet weight of 0.5 g containing empty plasmid or pET-22b/CsgA, and XG-0.5 and XG-1.0 stand for the adhesives prepared with *E. coli* cells containing pET-22b/CsgA-cp19k with wet weight of 0.5 g or 1.0 g) measured at a constant frequency of 10 Hz and 25 °C. **e**) Viscosity changes of XG and XG-cell bioadhesives from low shear rate (0.1 s^{-1}) to high shear rate (500 s^{-1}) at 25 °C.

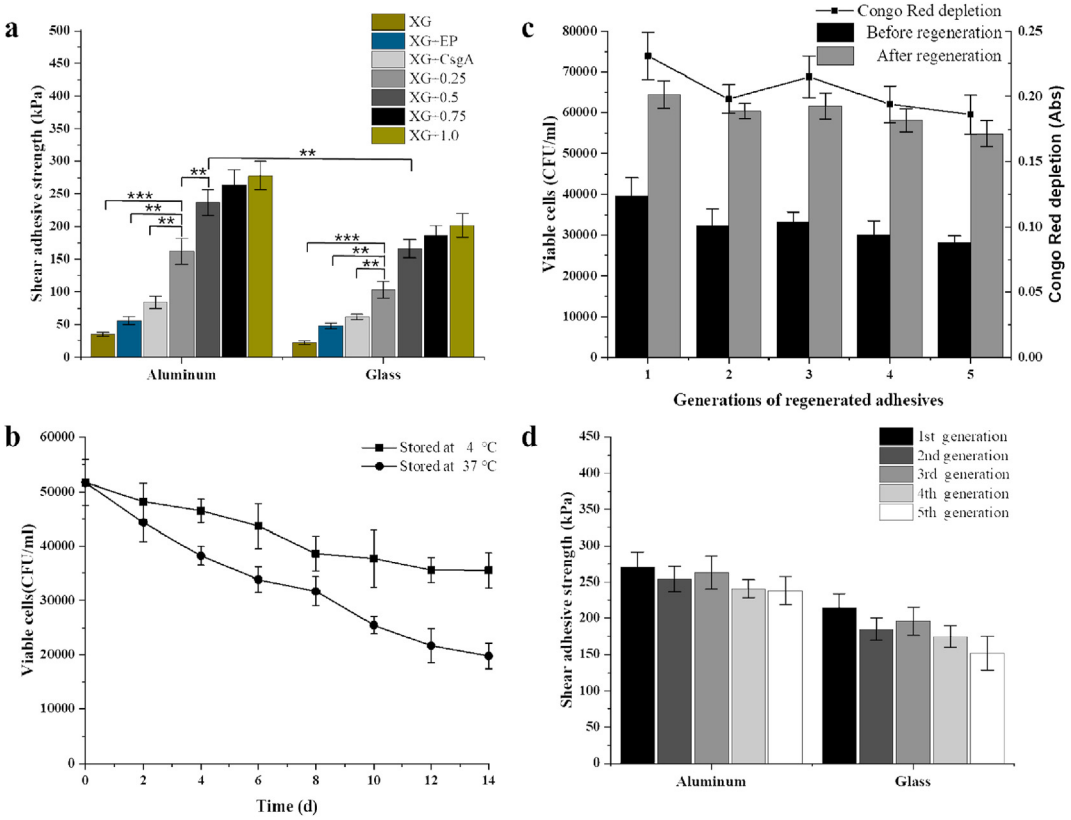

Fig. 6. The shear adhesive strength of bioadhesives were determined by lap shear test on a universal testing machine and the self-regeneration ability of bioadhesive was verified. **a**) Lap shear test of XG and XG-cell adhesive between aluminum or glass panels. XG-EP and XG-CsgA stand for the adhesives prepared with XG and *E. coli* cells with a wet weight of 0.5 g containing empty plasmid or pET-22b/CsgA. XG-0.25 to XG-1.0 stand for the adhesives prepared with *E. coli* cells containing pET-22b/CsgA-cp19k with wet weights from 0.25 g to 1.0 g. (**) $P < 0.01$, (***) $P < 0.001$. **b**) The CFU number of viable *E. coli* cells in the bioadhesive over time when stored at 4 °C or 37 °C. **c**) Detection of viable cell count and curli yield in 1–5 generations of regenerated adhesives. The CFU number of viable *E. coli* cells in the adhesives before and after regeneration detected by dilution coating plate method. **d**) The shear adhesive strength of the 1–5 generations of regenerated XG-cell adhesives between aluminum or glass panels.

that the cells displaying recombinant curli contributed to the surface coupling of the bioadhesive.

Rheological experiments proved that XG-cell gel exhibited a higher crosslinking density than XG gel, which helped to increase the cohesion of the adhesive, which may be one of the reasons for the enhanced adhesive strength of XG-cell gel. Interfacial coupling ability of cp19k is another important reason for the enhanced adhesive strength. cp19k possess a block copolymer-like sequence property, whose primary structure contains two alternating blocks which were believed to have a synergistic effect to promote interfacial adhesion force [31]. Among them, one block is dominated by Gly, Ser, Thr, Val and Ala residues containing large amounts of pendant amine or hydroxyl groups, which was believed to be favorable for the removal of surface-bound water layers and the interfacial couples to various foreign surfaces via hydrogen bonding, electrostatic interactions, hydrophobic interactions, etc. [11] The other block is rich in charged amino acids, which may participate in the formation of coordination bonds and help the adhesion of the metal interface. Moreover, the carboxyl and hydroxyl groups on the XG chain can also tightly bind to the interface, especially metals, through non-covalent interactions, which may also have a synergistic effect with cp19k [32].

The most attractive characteristics of living organism materials are viability and self-regeneration [33]. First, we proved that most of the *E. coli* cells can survive long-term in the bioadhesive when stored at low temperature (Fig. 6b). To examine regeneration performance, bioadhesives stored at 4 °C were passaged in LB broth supplemented with IPTG through five consecutive cycles of re-inoculation and growth. And the number of viable bacteria and curli yield in the adhesives before and after regeneration were detected (Fig. 6c). The results demonstrate the ability of live *E. coli* cells encapsulated in bioadhesive to self-regenerate and form curli under appropriate conditions. Further, we conjugated the regenerated cells with XG and used lap shear measurement to check the adhesive strength of the regenerated bioadhesive. The experimental results show that the 1–5 generations of regenerated adhesives still maintain a strong shear adhesive strength, proving the good reproducibility of the material (Fig. 6d).

4. Conclusions

The development of biomimetic adhesives based on the natural adhesion systems of marine organisms is rapidly progressing. Although some recombinant or native mfps based on mussel systems can achieve adhesion strengths of 300–500 kPa or higher, but these proteins can only be produced in milligram quantities, which is difficult to meet practical applications [34]. More importantly, these in vitro expressed proteins lack the unique self-assembly and self-regeneration properties of biological systems. The shear adhesion strength of the adhesives in this study was between 100 and 300 kPa, which was similar to the reported living cell adhesive based on mussel system [6]. However, the currently reported mussel-inspired living glue system relies on the action of tyrosinase, which requires the use of high concentrations of Cu (II) to ensure enzymatic activity, and thus may cause toxicity to living organisms in practical applications.

In this study, we have developed a novel living-cell bioadhesive by simulating the natural adhesion mechanism of barnacle cement and *E. coli* curli, using three self-assembly bioadhesive materials, cp19k, CsgA and XG. We have demonstrated that CsgA and cp19k fusion proteins have the ability to rapidly self-assemble into amyloid fibrils in a seawater environment. Amyloid fibrils can provide beneficial material properties such as resistance to degradation and mechanical strength, which allow the adhesive to remain stable in harsh environments. XG is a non-toxic natural material with good safety and biocompatibility, and its network structure gives the adhesive good thixotropy for easy pumping by injection and easy filling defects of any shape. In addition, the living cells in the bioadhesive endow it with the ability to regenerate itself. The adhesive we designed has low toxicity to organisms, strong resistance to the in vivo liquid environment, and easy pumpability, so it has potential applications in biomedical fields such as intestinal soft tissue repair. Based on flexible genetic engineering designs, we envision the future of making smart adhesives capable of environmentally-triggered repairs that could be used in a wider range of biomedical and industrial settings. For example, tissue repair by triggering adhesive regeneration in response to in vivo biochemical signals.

Credit author statement

Fei Li: Investigation, Writing – original draft, Writing – review & editing. Longyu Zhang: Methodology. Luona Ye: Software. Xiaoyan Li, Xiaoxiao Liu, Huanhuan Li, Jiarui Zhu, Huiming Pang: Validation. Yunjun Yan: Project administration, Funding acquisition. Li Xu, Min Yang: Resources, Supervision. Jinyong Yan: Conceptualization, Methodology.

Declaration of competing interest

The authors declare that they have no known competing financial interests or personal relationships that could have appeared to influence the work reported in this paper.

Acknowledgments

This work was supported by funding from the National Natural Science Foundation of China (NSFC32170090), Wuhan Morning Light Plan of Youth Science and Technology (2017050304010292), the Startup Fund for Talent Scholars of Huazhong University of Science and Technology (2016YXMS255) and the Fundamental Research Funds for the Central Universities (2020kfyXJJS119).

Appendix A. Supplementary data

Supplementary data to this article can be found online at https://doi.org/10.1016/j.mtbio.2022.100256.

References

[1] S. Ma, Y. Wu, F. Zhou, Bioinspired synthetic wet adhesives: from permanent bonding to reversible regulation, Curr. Opin. Colloid Interface Sci. 47 (2020) 84–98, https://doi.org/10.1016/j.cocis.2019.11.010.
[2] A.S. Mostaert, M.J. Higgins, T. Fukuma, et al., Nanoscale mechanical characterisation of amyloid fibrils discovered in a natural adhesive, J. Biol. Phys. 32 (5) (2006) 393–401, https://doi.org/10.1007/s10867-006-9023-y.
[3] Chao Zhong, et al., Strong underwater adhesives made by self-assembling multi-protein nanofibres, Nat. Nanotechnol. 9 (10) (2014) 858–866, https://doi.org/10.1038/nnano.2014.199.
[4] T.C. Tang, B. An, Y. Huang, et al., Materials design by synthetic biology, Nat. Rev. Mater. 6 (4) (2021) 332–350, https://doi.org/10.1038/s41578-020-00265-w.
[5] S.A. Tursi, Ç. Tükel, Curli-containing enteric biofilms inside and out: matrix composition, immune recognition, and disease implications[J], Microbiol. Mol. Biol. Rev. 82 (4) (2018), https://doi.org/10.1128/MMBR.00028-18 e00028-18.
[6] C. Zhang, J. Huang, J. Zhang, et al., Engineered Bacillus subtilis biofilms as living glues, Mater. Today 28 (2019) 40–48, https://doi.org/10.1016/j.mattod.2018.12.039.
[7] B. An, Y. Wang, X. Jiang, et al., Programming living glue systems to perform autonomous mechanical repairs, Matter 3 (6) (2020) 2080–2092, https://doi.org/10.1016/j.matt.2020.09.006.
[8] D.E. Barlow, G.H. Dickinson, B. Orihuela, et al., Characterization of the adhesive plaque of the barnacle Balanus amphitrite: amyloid-like nanofibrils are a major component, Langmuir 26 (9) (2010) 6549–6556, https://doi.org/10.1021/la9041309, 2010.
[9] Christian Wasmer, et al., Amyloid fibrils of the HET-s (218–289) prion form a β solenoid with a triangular hydrophobic core, Science 319 (5869) (2008) 1523–1526.
[10] K. Kamino, Molecular design of barnacle cement in comparison with those of mussel and tubeworm, J. Adhes. 86 (1) (2010) 96–110, https://doi.org/10.1080/00218460903418139.
[11] C.R. So, E.A. Yates, L.A. Estrella, et al., Molecular recognition of structures is key in the polymerization of patterned barnacle adhesive sequences, ACS Nano 13 (5) (2019) 5172–5183, https://doi.org/10.1021/acsnano.8b09194.
[12] C. Liang, J. Strickland, Z. Ye, et al., Biochemistry of barnacle adhesion: an updated review, Front. Mar. Sci. 6 (2019), https://doi.org/10.3389/fmars.2019.00565.

[13] L.A. Estrella, E.A. Yates, K.P. Fears, et al., Engineered Escherichia coli biofilms produce adhesive nanomaterials shaped by a patterned 43 kDa barnacle cement protein, Biomacromolecules 22 (2) (2020) 365–373, https://doi.org/10.1021/acs.biomac.0c01212.
[14] Y. Wang, B. An, B. Xue, et al., Living materials fabricated via gradient mineralization of light-inducible biofilms, Nat. Chem. Biol. 17 (3) (2021) 351–359, https://doi.org/10.1038/s41589-020-00697-z.
[15] A.Y. Chen, Z. Deng, A.N. Billings, et al., Synthesis and patterning of tunable multiscale materials with engineered cells, Nat. Mater. 13 (5) (2014) 515–523, https://doi.org/10.1038/nmat3912.
[16] P.E. Jansson, L. Kenne, B. Lindberg, Structure of the extracellular polysaccharide from Xanthomonas campestris, Carbohydr. Res. 45 (1) (1975) 275–282, https://doi.org/10.1016/S0008-6215(00)85885-1.
[17] G. Holzwarth, E.B. Prestridge, Multistranded helix in xanthan polysaccharide, Science 197 (4305) (1977) 757–759, https://doi.org/10.1126/science.887918.
[18] Z. Liu, P. Yao, Injectable thermo-responsive hydrogel composed of xanthan gum and methylcellulose double networks with shear-thinning property, Carbohydr. Polym. 132 (2015) 490–498, https://doi.org/10.1016/j.carbpol.2015.06.013.
[19] J. Patel, B. Maji, N.S.H.N. Moorthy, et al., Xanthan gum derivatives: review of synthesis, properties and diverse applications, RSC Adv. 10 (45) (2020) 27103–27136, https://doi.org/10.1039/D0RA04366D.
[20] Yu Jiang, et al., Multigene editing in the Escherichia coli genome via the CRISPR-Cas9 system, Appl. Environ. Microbiol. 81 (7) (2015) 2506–2514, https://doi.org/10.1128/AEM.04023-14.
[21] C. Reichhardt, A.N. Jacobson, M.C. Maher, J. Uang, O.A. McCrate, M. Eckart, et al., Congo red interactions with curli-producing E. coli and native curli amyloid fibers, PLoS One 10 (2015), e0140388, https://doi.org/10.1371/journal.pone.0140388.
[22] L. Cegelski, J.S. Pinkner, N.D. Hammer, et al., Small-molecule inhibitors target Escherichia coli amyloid biogenesis and biofilm formation, Nat. Chem. Biol. 5 (12) (2009) 913–919, https://doi.org/10.1038/nchembio.242.
[23] X. Wang, D.R. Smith, J.W. Jones, et al., In vitro polymerization of a functional Escherichia coli amyloid protein, J. Biol. Chem. 282 (6) (2007) 3713–3719, https://doi.org/10.1074/jbc.M609228200.
[24] Xingping Liu, et al., Amyloid fibril aggregation: an insight into the underwater adhesion of barnacle cement, Biochem. Bioph. Res. Co. 493 (1) (2017) 654–659, https://doi.org/10.1016/j.bbrc.2017.08.136.
[25] Benjamin A. Shoemaker, John J. Portman, Peter G. Wolynes, Speeding molecular recognition by using the folding funnel: the fly-casting mechanism, Proc. Natl. Acad. Sci. USA. 97 (16) (2000) 8868–8873, https://doi.org/10.1073/pnas.160259697.
[26] X. Wang, C. Wang, B. Xu, et al., Adsorption of intrinsically disordered barnacle adhesive proteins on silica surface, Appl. Surf. Sci. 427 (2018) 942–949, https://doi.org/10.1016/j.apsusc.2017.08.108.
[27] W.R. Glomm, Halskau Ø, A.M.D. Hanneseth, et al., Adsorption behavior of acidic and basic proteins onto citrate-coated Au surfaces correlated to their native fold, stability, and pI, J. Phys. Chem. B 111 (51) (2007) 14329–14345, https://doi.org/10.1021/jp074839d.
[28] Ao Wang, Sinan Keten, Adhesive behavior and detachment mechanisms of bacterial amyloid nanofibers. npj Computat, Mater 5 (1) (2019) 1–8, https://doi.org/10.1038/s41524-019-0154-7.
[29] C.R. So, J.M. Scancella, K.P. Fears, et al., Oxidase activity of the barnacle adhesive interface involves peroxide-dependent catechol oxidase and lysyl oxidase enzymes, ACS Appl. Mater. Interfaces 9 (13) (2017) 11493–11505, https://doi.org/10.1021/acsami.7b01185.
[30] X.T. Le, S.L. Turgeon, Rheological and structural study of electrostatic cross-linked xanthan gum hydrogels induced by β-lactoglobulin, Soft Matter 9 (11) (2013) 3063–3073, https://doi.org/10.1039/C3SM27528K.
[31] K. Kamino, Mini-review: barnacle adhesives and adhesion, Biofouling 29 (6) (2013) 735–749, https://doi.org/10.1080/08927014.2013.800863.
[32] F. Garcıa-Ochoa, V.E. Santos, J.A. Casas, et al., Xanthan gum: production, recovery, and properties, Biotechnol. Adv. 18 (7) (2000) 549–579, https://doi.org/10.1016/S0734-9750(00)00050-1.
[33] C.D. Ma, C. Wang, C. Acevedo-Vélez, et al., Modulation of hydrophobic interactions by proximally immobilized ions, Nature 517 (7534) (2015) 347–350, https://doi.org/10.1038/nature14018.
[34] R.J. Stewart, Protein-based underwater adhesives and the prospects for their biotechnological production, Appl. Microbiol. Biotechnol. 89 (1) (2011) 27–33, https://doi.org/10.1007/s00253-010-2913-8.